Study of ice transparency with IceCube flashers

Dmitry Chirkin for the IceCube collaboration

dima@icecube.wisc.edu

University of Wisconsin at Madison, Madison, USA

Abstract

The IceCube detector, planned to reach 1 km3 in the next 2 years, is now 68% complete with 59 strings deployed in the ice and 59 IceTop stations installed on the surface. To realize the full potential of the detector the properties of light propagation in the ice surrounding the detector must be known to the best achievable precision. While the model describing ice built in [1] provided an adequate description of ice in the AMANDA detector, it does not seem to extrapolate well to describe the photon propagation at larger distances within the IceCube detector. This report presents a new method of fitting the fully heterogeneous ice model to a data set of flasher events collected with IC40 in 10/08.

1 Flasher dataset

IceCube runs 111738-111744 of "request B" [2] contain data with each of DOMs 1-60 of string 63 of IC40 flashing in a sequence. For each of the flashing DOMs 250 flasher events were used. All 6 horizontal LEDs were switched on with maximum brightness and width, creating a pattern of light around string 63 that should be rather symmetric.
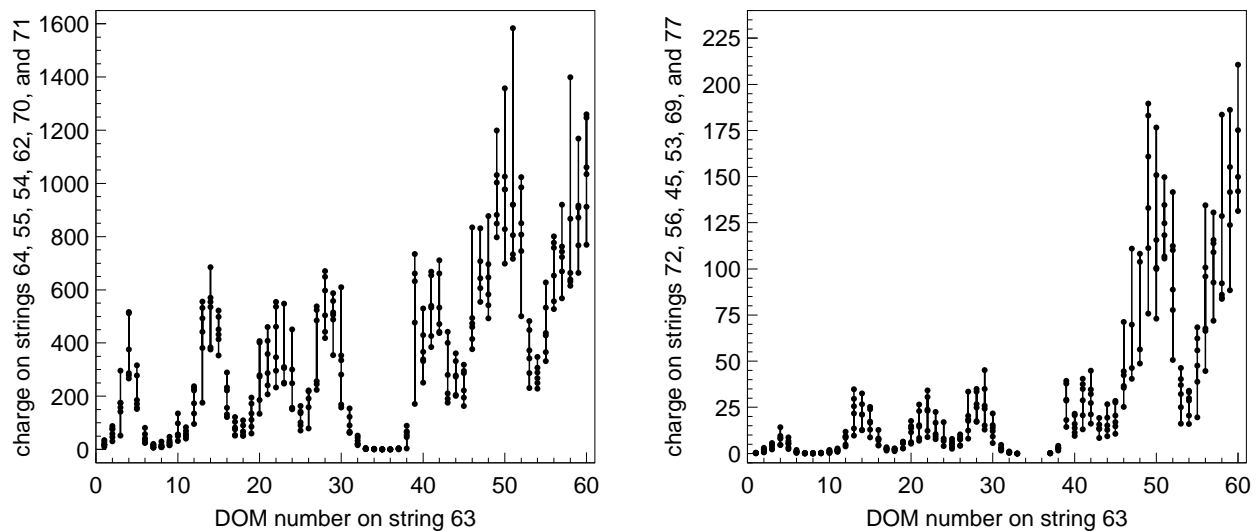

Figure 1: Charges on the six nearest strings (left) and six next-to-nearest strings (right), observed when flashing at the same position on string 63.

As seen in Figure 1 there is a substantial variation between the charges collected on the six surrounding strings. This variation can be due to variations in relative orientation of the flasher LEDs with respect to the surrounding strings; due to relative variation of light yield the between the different flasher LEDs, and due to some difference in distance to and depth of the six surrounding strings. The amount of variation due to these uncertainties can be quantified with an RMS of the deviation from the mean between the six surrounding strings, shown on Figure 2.

A multi-pulse extraction was applied to the data, using waveforms recorded by both ATWD and FADC. The resulting pulses were binned in 25 ns bins, from 0 to 5000 ns from the flasher pulse (extracted from ATWD channel 3 of the flasher DOM). Due to high number of saturated DOMs (with a variety of problems due to high received charge) and to minimize the effect of a particular selected angular sensitivity model (of a DOM) the photon data collected on string 63 was not used in the fit.

2 Six-parameter ice model

This section overviews the so-called six-parameter ice model introduced in [1].
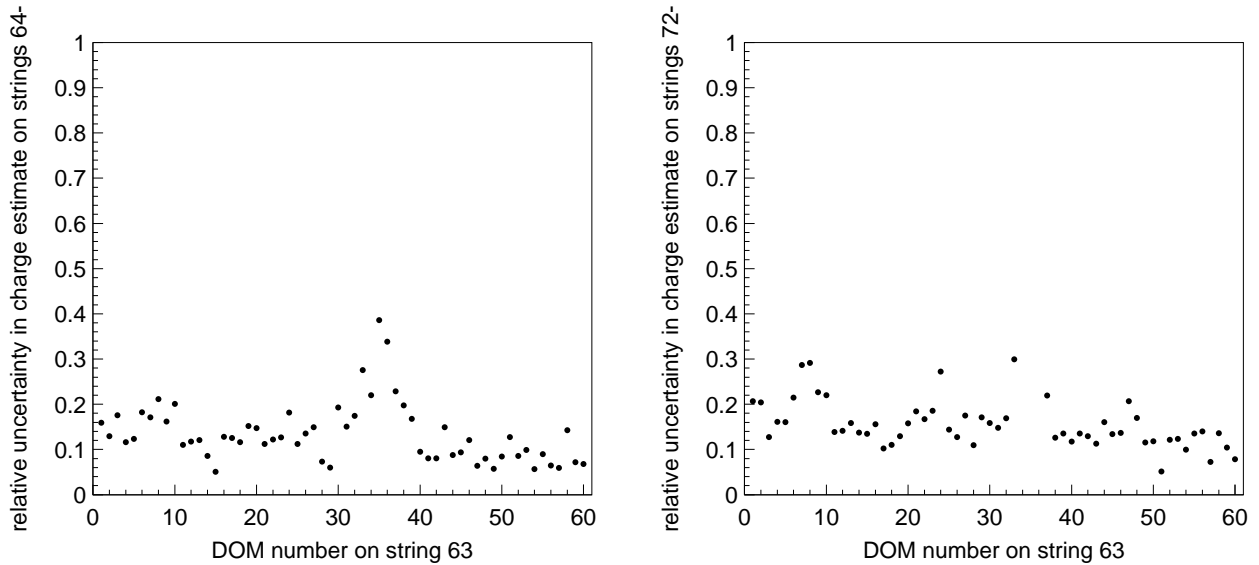
Figure 2: Relative uncertainty in the mean charge estimated from measured charges on the six nearest strings (left) and six next-to-nearest strings (right) observed when flashing at the same position on string 63.

The ice is described by a table of parameters $b_e(400)$, $a_{dust}(400)$, related to scattering and absorption at 400 nm, and temperature $\delta\tau$, given for each ice layer (assuming layers of 10-meter width), and by the six parameters (fitted previously to AMANDA data): α, κ, A, B, D, and E.

The scattering and absorption coefficients within the six-parameter ice model are given (for wavelength λ in nm) by the following expressions:

$$b_e(\lambda) = \frac{1}{\lambda_e} = b_e(400) \cdot \left(\frac{\lambda}{400}\right)^{-\alpha}$$

$$a(\lambda) = \frac{1}{\lambda_a} = a^*(400) \cdot \lambda^{-\kappa} + Ae^{-B/\lambda} \cdot (1 + 0.01 \cdot \delta\tau), \quad \text{with} \quad a^*(400) = D \cdot a_{dust}(400) + E.$$

This work fits only for the values of $b_e(400)$ and $a_{dust}(400)$ and relies on the six-parameter ice model to extrapolate scattering and absorption for wavelengths other than 405 nm (of the flasher LED light).

3 Simulation

60 flasher configurations (one for each of the DOMs flashing on string 63) need to be simulated very quickly, so that simulations based on many different sets of coefficients $b_e(400)$ and $a_{dust}(400)$ could be compared to the data.

A program called PPC (photon propagation code [3]) was written for this purpose. It propagates photons through heterogeneous ice described by the six-parameter ice model (based on a selected set of parameters $b_e(400)$ and $a_{dust}(400)$) until they hit a DOM or get absorbed. No special weighting scheme was employed, except that the DOMs were scaled up in size (a factor $5 - 16$, depending on the required timing precision[1]), and the number of emitted photons was scaled down by a corresponding factor ($5^2 - 16^2$).

Several different versions of the program were written: initial c++ code, somewhat faster (accelerated) c++ code, a complete program implementation in Assembly (for the 32-bit i686 with SSE2 architecture), and a version that employs the NVidia's GPUs (graphics processing units) via the CUDA interface. The relative performance of these different implementations (for simulating both flashers and Cerenkov light from muons) is compared in Table 1.

The writing of the GPU version of PPC was prompted by a similar project [4], which showed that acceleration factors ~ 100 compared to the CPU-only version were possible. After demonstrating the impeccable agreement between test

---

[1]A factor of 5 introduces the maximum error of (5-1) · 17.8 cm / 22 cm/ns=3.2 ns in the arrival time (for an OM with radius 17.8 cm and for speed of light in ice of 22 cm/ns). Assuming a flat distribution the rms is 3.2 ns/$\sqrt{3}$=1.9 ns. Respectively, a factor of 16 introduces an error with rms of no more than 7.0 ns. An additional consideration is a small loss of OM hit occupancy, which may occur for larger factors.

test	c++	fast c++	Assembly	GTX 295 GPU
flasher	1.00	1.33	2.39	142.
muon	1.00	1.87	3.43	263.

Table 1: Comparison in speed of different versions of PPC, as tested on the i7 920 (2.67 GHz) CPU

simulation sets made with the c++, Assembly, and GPU implementations of PPC, the GPU version was chosen for the following analysis on a GPU-enabled computer [5].
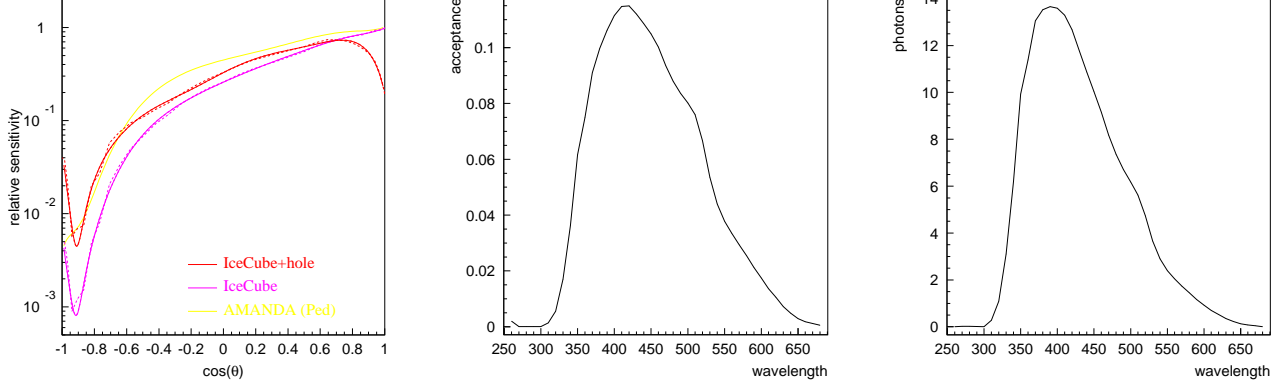

Figure 3: Angular sensitivity of an IceCube optical module, normalized to 1.0 at $\cos\theta = 1$ (left). Optical module acceptance: fraction of photons arriving along the PMT axis (at $\cos\theta = 1$) that are recorded (center). Number of Cerenkov photons (in 10 nm bins) emitted by one meter of bare muon track, convolved with the optical module acceptance (right). The integral count under this curve is 2107.84 photons.

The angular sensitivity of the IceCube optical module was modeled according to the "hole ice" description of [6], which is shown in Figure 3. The OM acceptance (including the glass and gel transmission, and PMT efficiency) was calculated according to [6] for an OM of radius 17.8 cm. At 405 nm (flasher center wavelength) the OM acceptance is 11.3% (reading off of Figure 3). The Cerenkov photons were sampled from the distribution shown in the right plot of Figure 3, which is a convolution of the OM acceptance curve with the Cerenkov photon spectrum given by the Frank-Tamm formula:

$$\frac{2\pi\alpha}{\lambda^2}\sin^2\theta_c d\lambda dl.$$

The "dressed" muon light production is treated via the use of the "effective length" dl, as described in the appendix A. The phase refractive index n_p used in the formula above (defining the Cerenkov angle $\cos\theta_c = 1/n_p$) and the group refractive index n_g (used in calculation of the speed of light in medium) were estimated according to formulae from [7]:

$$n_p = 1.55749 - 1.57988 \cdot \lambda + 3.99993 \cdot \lambda^2 - 4.68271 \cdot \lambda^3 + 2.09354 \cdot \lambda^4$$

$$n_g = n_p \cdot (1 + 0.227106 - 0.954648 \cdot \lambda + 1.42568 \cdot \lambda^2 - 0.711832 \cdot \lambda^3).$$

The angular distribution of photon scattering was modeled according to the Henyey-Greenstein function:

$$p(\cos\theta) = \frac{1}{2}\frac{1 - g^2}{[1 + g^2 - 2g \cdot \cos\theta]^{3/2}},$$

which can be analytically integrated and inverted to yield a $\cos\theta$ as a function of a random number $s = 2 \cdot P - 1 \in [-1; 1]$:

$$\cos\theta = \frac{1}{2g}\left(1 + g^2 - \left(\frac{1 - g^2}{1 + gs}\right)^2\right).$$

The value of $g = <\cos\theta> = 0.8$ was used as in [1]. Higher values (as high as ~ 0.94 [8]) are predicted by the Mie scattering theory, however, these result in slower simulation, while yielding almost unchanged values of the effective scattering $\lambda_e = \lambda/(1 - g)$ and absorption λ_a.

3

4   Likelihood description

Consider a single charge value (received by DOM i in time bin n when flashing DOM k) that is measured by taking data (with a total photon count of d in n_d flasher events and a per-event expectation of λ_d), and predicted by the simulation (again, with a total photon count of s in n_s simulated events and a per-event expectation of λ_s). Naively one expects the best approximations to λ_d and λ_s from data and simulated events to be $\lambda_d = d/n_d$, and $\lambda_s = s/n_s$.

Suppose the systematic error in describing data with simulation (i.e., describing λ_d with λ_s) is of the order of $\sigma \approx 10 - 20\%$. One quantifies the amount of disagreement between data and simulation in the presence of such an error with a $\chi^2_{i,n,k}$ (omitting the indices i, n, and k):

$$\chi^2 = \frac{(\log \lambda_d - \log \lambda_s)^2}{\sigma^2}.$$

This systematic error uncertainty can be modeled with a probability distribution function

$$\frac{1}{\sqrt{2\pi}\sigma} \exp \frac{-(\log \lambda_d - \log \lambda_s)^2}{2\sigma^2}.$$

Given that λ_d and λ_s are not known, and the measured values are d and s, one formulates the likelihood function that describes counts measured in both data and simulation as

$$\frac{(\lambda_s n_s)^s}{s!} e^{-\lambda_s n_s} \cdot \frac{(\lambda_d n_d)^d}{d!} e^{-\lambda_d n_d} \cdot \frac{1}{\sqrt{2\pi}\sigma} \exp \frac{-(\log \lambda_d - \log \lambda_s)^2}{2\sigma^2}.$$

Taking the log with a minus sign, this becomes:

$$F = \ln s! + \lambda_s n_s - s \log(\lambda_s n_s) + \ln d! + \lambda_d n_d - d \log(\lambda_d n_d) + \frac{1}{2\sigma^2} \log^2 \frac{\lambda_d}{\lambda_s} + \log(\sqrt{2\pi}\sigma).$$

The function $F(\lambda_s, \lambda_d)$ can be easily minimized against λ_s and λ_d, yielding estimates of these quantities. To demonstrate this, first the derivatives of F are calculated and set to 0:

$$\lambda_s \frac{\partial F}{\partial \lambda_s} = \lambda_s n_s - s - \frac{1}{\sigma^2} \log \frac{\lambda_d}{\lambda_s} = 0,$$

$$\lambda_d \frac{\partial F}{\partial \lambda_d} = \lambda_d n_d - d + \frac{1}{\sigma^2} \log \frac{\lambda_d}{\lambda_s} = 0.$$

The sum of these ($\lambda_s n_s + \lambda_d n_d = s + d$) yields an expression of λ_d as a function of λ_s. Plugging it into the first of the above two equations one gets

$$f = \lambda_s \frac{\partial F}{\partial \lambda_s}(\lambda_s, \lambda_d(\lambda_s)) = \lambda_s n_s - s - \frac{1}{\sigma^2} \log \frac{\lambda_d(\lambda_s)}{\lambda_s} = 0.$$

This equation can be solved with a few iterations of the Newton-Raphson method starting with a solution to

$$\lambda_s = \lambda_d(\lambda_s): \qquad \lambda_s = \lambda_d = \frac{s + d}{n_s + n_d}.$$

At each iteration the value of λ_s is adjusted by $-f/f'$, where the derivative is easily evaluated as

$$f' = n_s \left(1 + \frac{1}{\sigma^2}(\frac{1}{\lambda_s n_s} + \frac{1}{\lambda_d n_d}) \right).$$

Once the likelihood function is solved for the best values of λ_s and λ_d, these can be plugged into the $\chi^2_{i,n,k}$ above. One can now write the complete χ^2 function (adding the regularization terms R_j described in the next section) as a sum over all DOMs i and time bins n, when flashing DOMs k:

$$\chi^2 = \sum_{i,n,k} \frac{(\log \lambda_d - \log \lambda_s)^2}{\sigma^2} + \sum_{1,2} \alpha_j R_j.$$

5 Regularization terms

Two regularization terms are added to the likelihood function described in the previous section. The first one intends to minimize the unwanted fluctuations of scattering and absorption coefficients with depth and is formed of second derivative terms:

$$R_r = \sum_{i=2}^{N-1} \left[(\log b_e[i-1] - 2 \cdot \log b_e[i] + \log b_e[i+1])^2 + (\log a^*[i-1] - 2 \cdot \log a^*[i] + \log a^*[i+1])^2 \right].$$

Here N is the number of ice layers in which b_e and a^* are defined.

The second term intends to minimize the unwanted fluctuations in the diagram of a^* vs. b_e. It is constructed as an excess of the sum of distances between the consecutive points $(\log b_e, \log a^*)$ over the shortest distance connecting the end points:

$$R_u = -D(1, N) + \sum_{j=1}^{N-1} D(j, j+1), \quad \text{where} \quad D(j_1, j_2) = \sqrt{(\log b_e[j_1] - \log b_e[j_2])^2 + (\log a^*[j_1] - \log a^*[j_2])^2}.$$

The points $(\log b_e, \log a^*)$ are sorted by the value of $\log b_e + \log a^*$ and shown in the above sum with the index $j[i]$.

6 Fitting the data

The six horizontal flashers on a single board flashing at maximum brightness and width emit $\sim 4.5 \cdot 10^{10}$ photons [9] (at room temperature in the lab, without the surrounding DOM glass sphere). Only 11.3% of these, or $5.085 \cdot 10^9$, remain after accounting for the OM acceptance (as explained in section 3). Using a DOM size scaling factor of 16 only $1.986 \cdot 10^7$ photons need to be simulated.

A base number 9765625 of simulated photons with a scaling factor of 16 corresponds to $2.5 \cdot 10^9$ photons without scaling (i.e., OM size scaling factor of 1.0), or $2.212 \cdot 10^{10}$ real photons leaving the flasher DOM (after accounting for the receiving OM acceptance). This is a "unit bunch" of photons, which is simulated in ~ 1 second on a single GPU of [5].

In the following a "photon yield factor" p_y is the number of unit bunches that correspond to a given number of photons. E.g., $4.5 \cdot 10^{10}$ photons emitted by a flasher board correspond to a photon yield factor of $p_y = 2.034$. This represents the upper limit on the photon yield factor since a fraction of photons is likely absorbed by the DOM glass sphere or reflected back when escaping the flasher DOM.

For a given p_y, starting with the bulk values of $b_e(400) = 0.046$ and $a_{dust}(400) = 0.044$ the minimizer converges in ~ 20 steps. At each iteration step the values of b_e and a^* are varied in consecutive ice layers. Five flashing DOMs closest to the layer, which properties are varied, are used to estimate the variation of the χ^2 when b_e and a^* are changed 4 times (4 combinations of $b_e \pm \delta b_e$ and $a^* \pm \delta a^*$). Figure 4 shows ice properties after each of 20 steps of the minimizer.

This minimization procedure is run for different values of p_y, and the average χ^2 of the final few steps of the minimizer is shown in Figure 5. The best fit is achieved for $p_y = 1.9 \pm 0.2$, which is just below the p_y value of the average photon yield measured in the lab. Since the best value of p_y is calculated by the method itself, the resulting table of $b_e(400)$ and $a^*(400)$ is independent of a possible constant scaling factor in the charge estimate.

Further constraint can be placed on the best value of p_y if one considers DOMs on string 63, which recorded charge substantially exceeds the simulated charge (see Figure 5). The DOMs that received high charge should show saturation or loss of recorded charge due to inability of the system to cope with large stream of data from string 63. Either way their charge should not exceed that estimated in the simulation (which did not account for saturation). As explained in section 1 string 63 DOMs were not used in the fit, so using them in this manner provides a rather independent confirmation of the found value of p_y.

The difference between the (shades of) green curves of Figure 5, showing the ice properties for $p_y = 1.7 - 2.1$, corresponds to $\pm 1\sigma$ uncertainty in the measured ice properties. This uncertainty grows in the dust layer (this might be improved with more simulation), and, quite naturally, at depths above and below the detector. It is possible to bias the fit at these depths towards the values previously measured or extrapolated in [1] by seeding the minimizer with values of $b_e(400)$ and $a^*(400)$ from [10].

Data from all pairs of emitter-receiver DOMs (located in the same or different ice layers) contributed to the fit, unlike in the approach of [1], where only emitters and receivers at similar depths were used in the fits. Two fit strategies were tried in fitting the data: (a) the χ^2 was constructed with one term from each emitter-receiver pair (using the full received charge),
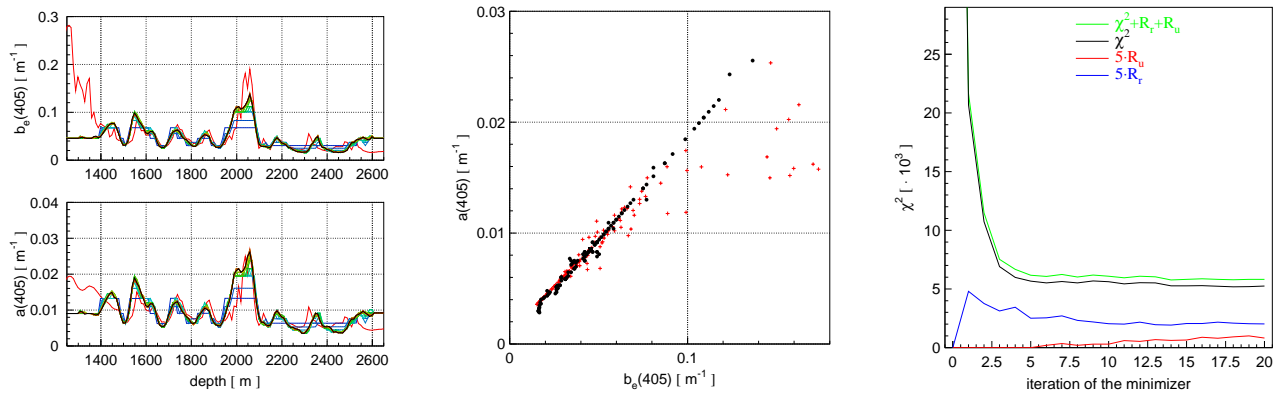
Figure 4: Values of $b_e(405)$ and $a(405)$ vs. depth after 20 steps of the minimizer (left). On this and the next plot red is nominal AHA ice [10], black is the fitted values after the last step of the minimizer. Correlation plot of $a(405)$ vs. $b_e(405)$ (center). χ^2 values achieved after each step of the minimizer (right). The starting value for the bulk ice is $1.12 \cdot 10^5$.
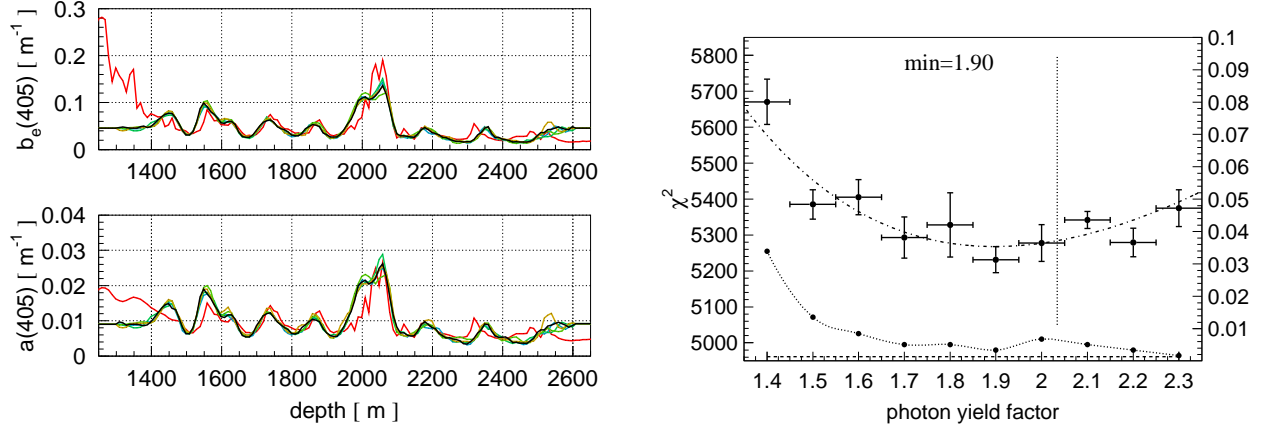

Figure 5: Values of $b_e(405)$ and $a(405)$ vs. depth for converged solutions at $p_y = 1.70 - 2.10$ (shades of green) and $p_y = 1.90$ (black). Red is the nominal AHA (left). Average χ^2 of the last steps of the minimizer at several values of p_y and the fitted log-normal curve with the minimum at $p_y = 1.90$ (right). The vertial dotted line at $p_y = 2.034$ corresponds to the average photon yield measured in the lab. The points of the lower curve (with a vertical scale on the right) show the fraction of DOMs on string 63 (which was not used in the fit) with charges greater than 100 that exceed the simulated values by more than 3σ. The dashed horizonal line shows the expected value of this fraction for purely statistical errors.

and (b) the χ^2 was constructed using recorded charge binned in 25 ns steps. Although (b) used the available information more fully, (a) turned out to be less susceptible to various problems in recorded waveforms, described in [11] and more robust with respect to fluctuations in the constructed χ^2 (between the simulated sets). Therefore, (a) was used for the final fit.

7 Comparison of the new fitted ice with nominal AHA [10]

Figure 6 demonstrates the improvement in description of the flasher data with the new model. Figure 7 shows data and simulation of the tilted flashers (which were not used in the fit of this work). Figure 8 shows that the agreement of the background muon simulation with data is much improved as well. Finally, Figure 9 shows a comparison of recorded charge for the standard candle [12], and a comparison in N_{ch} for all IceCube light sources. Many more plots are available at [13].
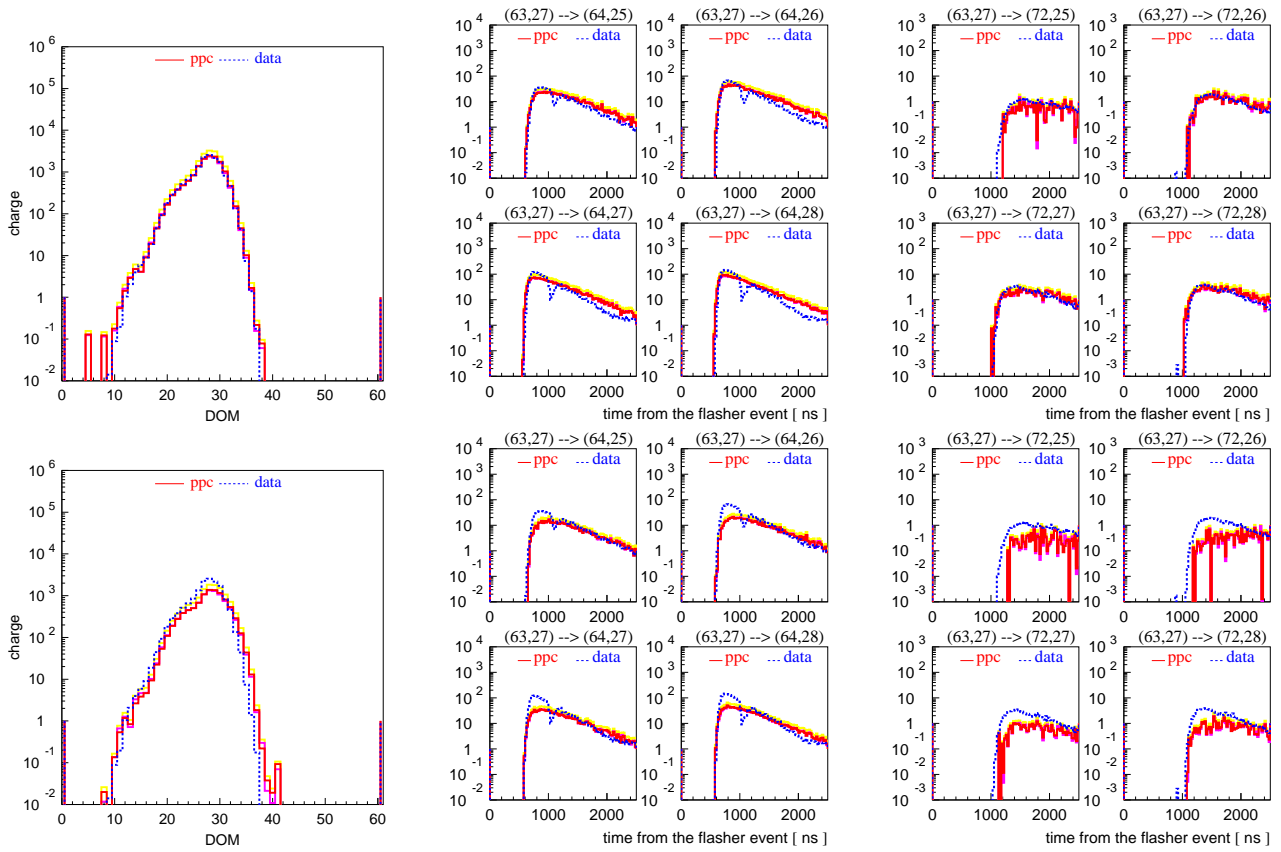
Figure 6: Top plots: ice model of this work, bottom plots: nominal AHA. Charges received on 6 nearest strings when DOM 63-27 was flashing (left), timing distributions on 4 DOMs closest in depth to the flashing DOM 63-27 on 6 nearest strings (center) and 6 next-to-nearest strings (right). The dip in the timing distributions is visible at high received charges and corresponds to the transition region between the part of the waveform captured with ATWD (first ∼ 450 ns) and FADC.
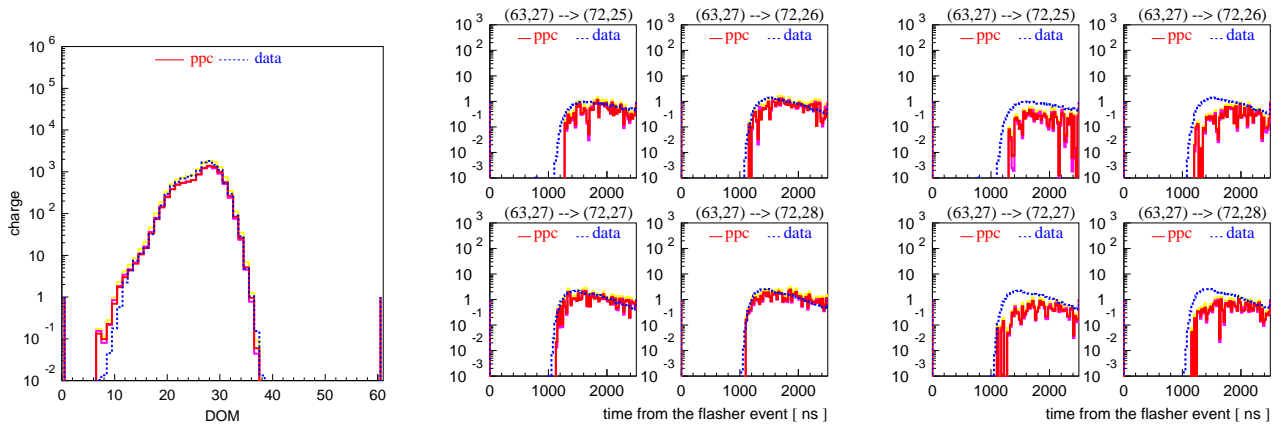

Figure 7: Charges received on 6 nearest strings when tilted LEDs on DOM 63-27 were flashing (left) and timing distributions on 4 DOMs closest in depth to the flashing DOM 63-27 on 6 next-to-nearest strings (center), both compared with the ice model of this work, and a comparison of the latter with AHA (right).
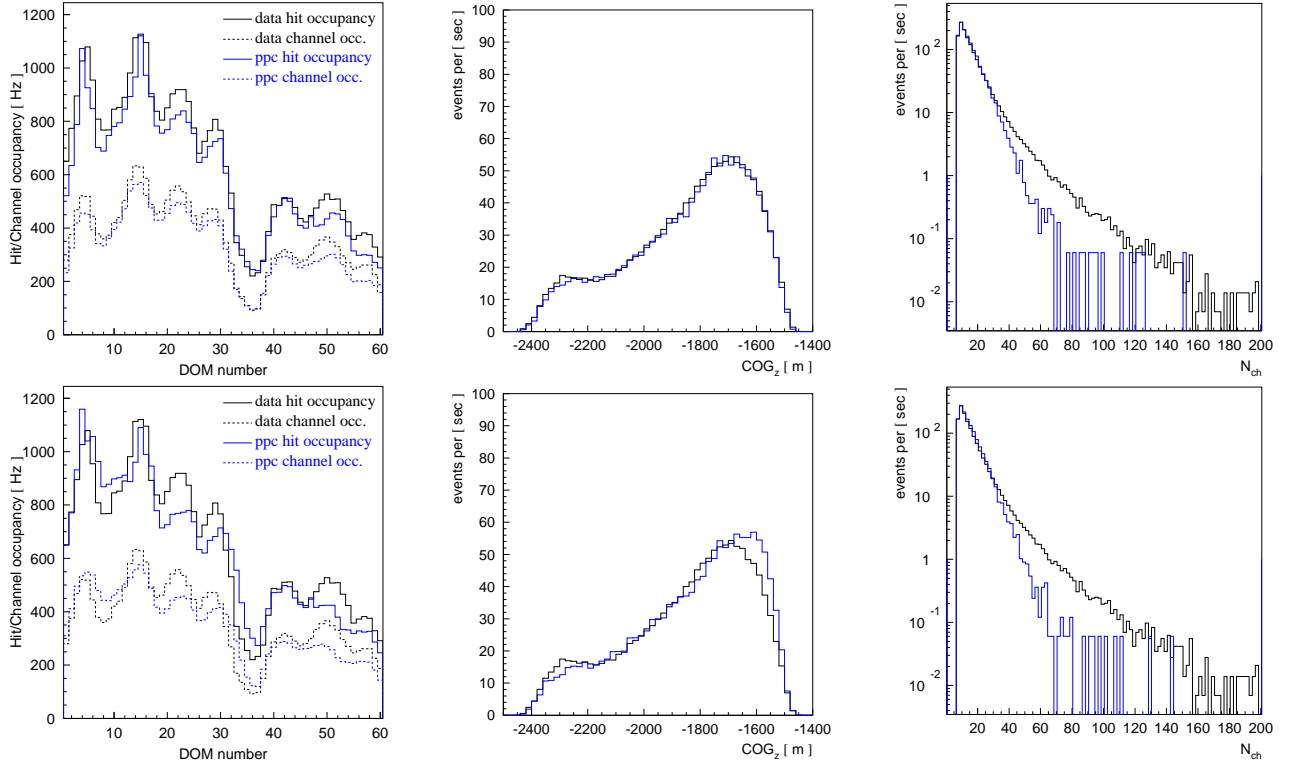
Figure 8: Top plots: ice model of this work, bottom plots: nominal AHA. OM hit and channel occupancies (left), COG_z (center) and N_{ch} distribution (right). The N_{ch} distribution is softer in the simulation due to lack of muon bundles (only single muons were simulated for this test).

A   Muon and cascade light production

The light yield of the muon and all of its secondaries (ionization and delta electrons, bremsstrahlung, electron pair production, and photonuclear interaction) with energies below 500 MeV (the e_{cut} of MMC [14] in the detector region) is parametrized by substituting the length of the Cerenkov light-emitting segment of a "bare" muon dl with [15]

$$dl \cdot \left(1.172 + 0.0324 \cdot \log_e\left(E\,[\text{GeV}]\right)\right).$$

The light yield of cascades is also parametrized via the use of the "effective length" [15]:

$$dl = 0.894 \cdot 4.889 \text{ m/GeV} \cdot E\,[\text{GeV}] \qquad \text{for electromagnetic cascades}$$
$$dl = 0.860 \cdot 4.076 \text{ m/GeV} \cdot E\,[\text{GeV}] \qquad \text{for hadronic cascades.}$$

Newer parametrization exists [16], but was not used in this work.

B   Acknowledgments

References

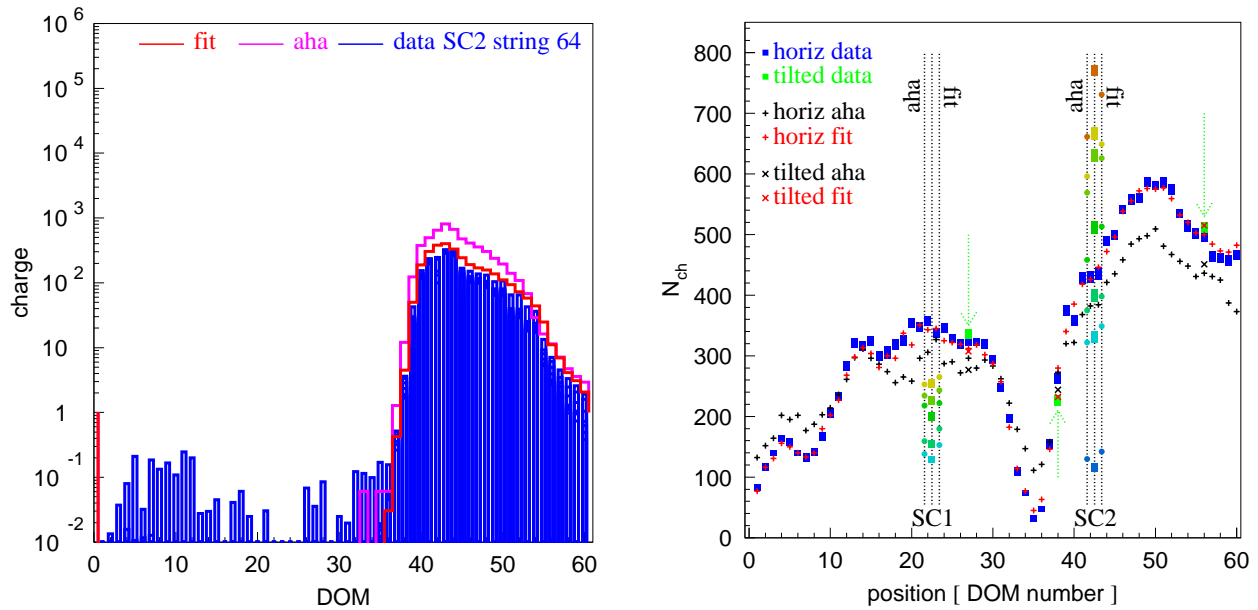[1] Optical properties of deep glacial ice at the South Pole M. Ackermann, et al., J. Geophys. Res. 111 (2006) D13203

Figure 9: Standard candle II data: blue, comparison with aha (scaled by x 0.5) and ice model of this work (scaled by x 0.25) (left). Comparison of average N_{ch} in data and simulation between horizonal flashers, tilted flashers, and standard candles I and II (right). Simulation of standard candles was scaled by same factors as in the figure on the left. The scaling implies that the light yield of the standard candles is overestimated by a factor $2 - 4$, or the DOM acceptance (3.04% read off Figure 3) is overestimated, or the scaling of ice properties with wavelength of [1], used to extrapolate scattering and absorption from 405 to 337 nm, is incorrect.

[2] Flasher data sets: http://wiki.icecube.wisc.edu/index.php/Flasher_Reconstruction

[3] PPC (all versions): http://icecube.wisc.edu/~dima/work/WISC/ppc/

[4] http://wiki.icecube.wisc.edu/index.php/GPU_based_implementation_of_Photon_Transport by Tareq Abuzayyad

[5] i7 920 (2.67 GHz) CPU computer with 3 GTX 295 NVidia cards (6 GPUs)

[6] efficiency.h file of photonics

[7] Role of Group and Phase Velocity in High-Energy Neutrino Observatories,
P. B. Price and K. Woschnagg, Astropart. Phys. 15 (2001) 97

[8] Mie scattering code and plots: http://icecube.wisc.edu/~dima/work/ICESCA/

[9] http://wiki.icecube.wisc.edu/index.php/Flashers

[10] AHA: Additionally Heterogeneous Absorption model, http://wiki.icecube.wisc.edu/index.php/New_ice_model

[11] http://wiki.icecube.wisc.edu/index.php/String_48_flasher_runs:_MPE_vs_SPE

[12] http://wiki.icecube.wisc.edu/index.php/Standard_Candle

[13] http://icecube.wisc.edu/~dima/work/WISC/ppc/fit/

[14] Muon Monte Carlo (MMC): http://icecube.wisc.edu/~dima/work/MUONPR/

[15] C.H.Wiebusch, Ph.D. thesis, Physikalische Institute, RWTH Aachen, 1995, pages 92-96.
The caption within Figure 7.56 (B) is correct, with LOG(E) understood as $\ln(E) \equiv \log_e(E)$

[16] M. Kowalski, On the Cerenkov light emission of hadronic and electro-magnetic cascades,
AMANDA internal report 20020803 (available from http://internal.icecube.wisc.edu/reports/amanda/).